Oxid Met (2013) 80:363–387
DOI 10.1007/s11085-013-9378-y

ORIGINAL PAPER

Oxidation of Slurry Aluminide Coatings on Cast Stainless Steel Alloy CF8C-Plus at 800 °C in Water Vapor

J. A. Haynes · B. L. Armstrong · D. Kumar · S. Dryepondt · Y. Zhang

Received: 17 August 2012 / Revised: 31 January 2013 / Published online: 20 February 2013

Abstract A new, cast austenitic stainless steel, CF8C-Plus (CF8C-P), has been developed for a wide range of high temperature applications, including diesel exhaust components, turbine casings and turbocharger housings. CF8C-P offers significant improvements in creep rupture life and creep rupture strength over standard CF8C steel. However, at higher temperatures and in aggressive environments such as those containing significant water vapor, an oxidation-resistant protective coating will be necessary to extend service life. The oxidation behavior of alloys CF8C and CF8C-P with various aluminide coatings were compared at 800 °C in air plus 10 vol% water vapor. Due to their affordability, slurry aluminides were the primary coating system of interest, although chemical vapor deposition and pack cementation coatings were also compared. Additionally, a preliminary study of the low-cycle fatigue (LCF) behavior of aluminized CF8C-P was conducted at 800 °C. Each type of coating provided substantial improvements in oxidation behavior, with simple slurry aluminides exhibiting very good oxidation resistance after 3,000 h testing in water vapor. Preliminary LCF results indicated that thicker aluminide coatings degraded high temperature fatigue properties of CF8C-P, whereas thinner coatings did not. Results suggest that appropriately designed slurry aluminide coatings are a viable option for economical, long-term oxidation protection of austenitic stainless steels in water vapor.

Keywords Stainless steel · Aluminide · Slurry coating · Water vapor · Oxidation

J. A. Haynes (✉) · B. L. Armstrong · D. Kumar · S. Dryepondt
Oak Ridge National Laboratory, Bethel Valley Road, Oak Ridge, TN 37831-6063, USA
e-mail: haynesa@ornl.gov

Y. Zhang
Department of Mechanical Engineering, Tennessee Technological University, Cookeville, TN 38505, USA
e-mail: YZhang@tntech.edu

Introduction

Alloy CF8C-Plus (CF8C-P) is a new grade of heat- and corrosion-resistant cast austenitic stainless steel, jointly developed by Oak Ridge National Laboratory (ORNL) and Caterpillar Inc. (Peoria, IL). The CF8C-P alloy has demonstrated substantial improvements over standard grade CF8C steel in high temperature strength and in resistance to creep, fatigue, thermal fatigue and aging [1]. Substantial quantities of CF8C-P have been commercially cast since 2007 for use in the exhaust systems of on-highway diesel engines [2, 3].

The alloy was created by adding Mn and N to the standard CF8C steel grade. The Mn addition improves castability and increases solubility for N, with both Mn and N acting synergistically to boost alloy mechanical properties [4, 5]. This alloy is reported to have twice the creep resistance of CF8C steel, with creep rupture properties that compare well with the much higher cost Ni-base alloys such as 617 [1, 3]. CF8C-P does not require additional heat treatments and demonstrates the best mechanical properties in the as-cast condition.

Due to its advanced high temperature properties and low cost relative to Ni-based alloys, CF8C-P is now being considered for more aggressive high temperature applications, including turbocharger housings, gas turbine casings and high temperature structural components for next generation coal-fired steam power generation facilities. Temperatures for potential applications range from 700 to 900 °C, with environments varying from slightly reducing to highly oxidizing in water vapor. However, preliminary studies have indicated that when significant water vapor is present the corrosion and oxidation resistance of CF8C-P are not adequate at temperatures of 750 °C and higher. Most high temperature stainless steels depend on the formation of Cr-containing oxide scales for oxidation resistance, but their protective capacity degrades rapidly in higher temperature environments containing water vapor [6, 7]. This is of significant concern for CF8C-P, since most combustion and exhaust applications generate water vapor.

Coatings that form protective Al_2O_3 scales, which are more stable than Cr_2O_3 in water vapor, and have been used for decades to improve the environmental resistance of selected high temperature Fe- and Ni-based alloys [8–11]. Only limited oxidation studies of chemical vapor deposition (CVD) aluminide coatings [3], pack cementation (PC) coatings and a commercial slurry coating [12] have previously been conducted on alloy CF8C-P.

The goal of this study was to evaluate the oxidation behavior of low cost slurry aluminide coatings on alloy CF8C-P in an aggressive environment containing 800 °C air plus 10 vol% H_2O. Three types of aluminide coatings (slurry, CVD and PC) were fabricated on cast CF8C-P and/or cast standard CF8C stainless steels in order to evaluate and compare coating performance during oxidation in water vapor. Slurry aluminideswere the coating of primary interest, due to their economic viability for steels and their previously demonstrated capacity to provide long-term oxidation protection to ferritic-martensitic steels in steam [13–15]. Additionally, a preliminary evaluation of the low-cycle fatigue (LCF) behavior of bare and coated CF8C-P at 800 °C was included.

Materials and Methods

Various types of aluminide coatings were fabricated on coupons (10 × 19 × 1.1 mm) electro-discharge machined from as-cast standard alloy CF8C and from as-cast alloy CF8C-P. Alloy compositions were measured by inductively coupled plasma (ICP), combustion, and inert gas fusion (IGF) analysis. Compositions of the two alloys are compared in Table 1. The CF8C-P alloy had lower N than targeted.

Slurry Aluminizing

The majority of coatings in this study were fabricated via slurry aluminizing, since that was the coating system of primary interest. Simple aluminum (Al) coatings were deposited using a slurry process developed at ORNL. The Al powder (Atlantic Equipment Engineers, Bergenfield, NJ) had an average particle size of $\sim$5.8 μm and surface area of 0.946 m^2/g, determined using dynamic light scattering (Horiba, Inc., Kyoto, Japan) and B.E.T. (Brunauer-Emmett-Teller analysis, Autosorb-1, Quantachrome Instruments, Boynton Beach, FL), respectively. The Al powder was mixed with an organic solvent and a dispersant in a ball mill for 4 h. After milling, a binder was added to the suspension, and the resulting mixture was rolled for an additional 24 h.

Alloy coupons were ground to a 600 grit finish and ultrasonically cleaned in ethanol prior to coating. Coupons of alloys CF8C and CF8C-P were dipped into the slurry suspension manually. Dip-coated samples were dried under ambient conditions and diffusion annealed in either ultra high purity (UHP) Ar or in vacuum plus UHP Ar.

Table 1 Compositions of substrate alloys

	CF8C		CF8C-P		CF8C-P nominal [1]
	wt%	at.%	wt%	at.%	wt%
Fe	68.1	66.9	62.3	61.3	Bal.
Cr	19.1	20.1	19.4	20.5	19.0
Ni	9.4	8.8	12.3	11.5	12.5
Mn	1.1	1.1	3.8	3.8	4.0
Si	1.1	2.2	0.5	1.0	0.5
Mo	0.3	0.2	0.2	0.1	0.3
Nb	0.8	0.5	0.6	0.4	0.8
Cu			0.1	0.04	
W			0.4	0.1	
C[a]	0.07	0.3	0.1	0.4	0.10
N[b]			0.1	0.3	0.25
S[a]			0.003	0.0	

[a] Measured by combustion analysis

[b] Measured by IGF analysis

Diffusion annealing of the slurry coatings included a heating rate of 3 °C/min to the annealing temperature (900 or 1,000 °C) in a horizontal tube furnace, a hold for the specified annealing time (0.5–6 h), followed by a natural furnace cool. Furnace pressure during annealing was 81.3 kPa (610 torr) under flowing UHP Ar (100 cm^3/min).

Pack Cementation

Pack aluminizing of select alloys was conducted at Tennessee Technological University (TTU). Coupons were ultrasonically cleaned in water and acetone prior to coating. The pack contained 20 wt% Cr–15 wt% Al master alloy (99.5 %, <100 mesh; Cerac, Inc.), 2 wt% NH_4Cl activator (99.999 %, <10 mesh), and the balance inert Al_2O_3 filler (99.5 %, 100–200 mesh).

Steel coupons were hung in a slotted alumina tube, which was loaded into an alumina crucible where the tube was surrounded by the powder mixture. The sealed crucible was inserted into an alumina reaction tube (~70-mm ID), which was positioned in a resistance-heated tube furnace. Ultra-high purity Ar (99.999 %) was used to purge the reaction chamber, and the furnace was heated to ~100 °C and held for 3 h to further remove moisture from the pack. The temperature was then raised to 900 °C, held for 6 h at 0.4 Pa (3×10^{-3} torr), and furnace cooled. Coating time was defined as the time at the aluminizing temperature.

Chemical Vapor Deposition

CVD of aluminide coatings on alloys CF8C and CF8C-P was conducted at ORNL in an ultra-high purity laboratory-scale CVD reactor. The reactor and CVD process are described in detail elsewhere [16]. Coupons were aluminized in flowing $AlCl_3 + H_2$ for 6 h at a CVD reactor temperature of 900 °C and a reactor pressure of 13.3 kPa. These conditions provided a low activity CVD process, which has been shown to result in an outward growing single-phase coating of either β-(Fe,Ni)Al or $(Fe,Ni)_3Al$ on 304L and 316 stainless steels [11, 16–19].

Cyclic Oxidation Testing in Water Vapor

Furnace cyclic oxidation testing was conducted at 800 °C in humid air (10 vol% H_2O) with a 100 h time at temperature per cycle. After each 100 h interval, specimens were removed from the hot furnace and allowed to air cool to room temperature in ambient air prior to weighing. The humidity level was controlled by atomizing distilled water into dry air flowing at 450 cm^3/min through an alumina tube inside a resistively-heated horizontal tube furnace. Details of the experimental set up can be found elsewhere [20].

Low-Cycle Fatigue Testing

Strain controlled LCF tests at 800 °C with a strain range of 0.5 % in laboratory air were performed on uncoated as-cast CF8C-P, uncoated CF8C-P annealed at 0.5 h and 6 h at 900 °C in vacuum, and as-cast CF8C-P coated with various aluminides.

The strain was applied at a strain rate of 0.05 % per second using a symmetrical triangular wave form, $R_\varepsilon = -1$. Both the uncoated and coated samples were of cylindrical shape with 6.4 mm gauge diameter and 19 mm gauge length. The test specimens were machined so that machining marks in the gauge portion of samples were parallel to the stress axis. The average roughness (R_a) of the gauge section, as measured by optical-profilometry, was ~ 1 μm for the bare alloy. A servo-hydraulic machine and an induction heater were used for fatigue testing. The temperature gradient along the gauge length was monitored by three K-type thermocouples attached to the gauge length, and was within ±5 °C for the test duration. A strain gauge-type extensometer with ceramic arms was used to measure the axial strain and to provide feedback control. One of each type specimen was tested in this preliminary fatigue study.

Characterization

Selected coatings were examined by optical microscopy, X-ray diffraction (XRD), scanning electron microscopy (SEM, Hitachi S3400) and electron probe micro-analysis (EPMA, JEOL 8200 Superprobe) with pure metal standards using wavelength dispersive X-ray spectroscopy (WDS) at 15 kV.

Results

Characterization of As-Fabricated Slurry Aluminide Coatings

All types of slurry coating in this study were continuous and exhibited no spallation or only minimal edge or corner spallation before and after oxidation testing. The slurry Al particles melted during annealing, forming a continuous, temporary liquid surface layer that inter-diffused with the underlying austenitic steel to form a solid multi-layer coating.

Figure 1a–f compares back scattered electron (BSE) images of metallographic sections of slurry coatings on CF8C and CF8C-P annealed at 900 °C for 0.5 h, 900 °C for 6 h, and 1,000 °C for 2 h. All slurry coatings resulted in two layers: (1) an outer layer (OL) of aluminide with a rough, irregular surface, and (2) a dense underlying interdiffusion zone (IDZ) containing numerous small precipitates of varying types. The OL showed minor amounts of vertical through-cracking, depending on coating thickness, Al content and alloy composition. Coatings with higher Al content had lower ductility, and contained more cracks, as expected. The vertical cracks did not extend past the OL–IDZ interface. Similar vertical through-cracks were reported to be inherent in Fe_2Al_5 slurry aluminides on ferritic-martensitic steel [13, 21], which survived 40 kh of steam testing at 650 °C without crack propagation into the IDZ [15].

There were varying degrees of fine Kirkendall-type porosity along the OL–IDZ interface, which has also been reported elsewhere [15]. Interfacial porosity increased with increasing temperature and time, and varied with alloy composition. Slurry coatings on CF8C and CF8C-P annealed at 900 °C/0.5 h showed little

porosity along the interface but greater amounts of cracking (Fig. 1a, b). Coatings annealed for longer times at 900 °C (6 h) had significant increases in porosity (Fig. 1c, d), with coatings on alloy CF8C displaying greater interfacial pore volume than those on CF8C-P. A further increase in interface porosity was observed on coatings annealed for 2 h at 1,000 °C (Fig. 1e, f), with coatings on CF8C again showing substantially greater pore volume than on CF8C-P. Interfacial porosity on CF8C was near continuous in some areas after 2 h at 1,000 °C (Fig. 1e).

XRD of various diffusion annealed slurry coatings indicated that the OL was of either the $(Fe,Ni)_3Al$ or β-(Fe,Ni)Al type structure (the XRD pattern d-spacings fit well with both phases). Table 2 compares the Al and Cr compositions (as measured by EPMA), averaged across the OL and IDZ, along with the measured thickness of each layer. The average Al content of the OL ranged from ~30 to ~49 at.% (Table 2), depending on annealing conditions. When combined with the measured Al contents, the XRD patterns suggest a hypostoichiometric β-(Fe,Ni)Al structure for the as-fabricated OL. The exception was the 1,000 °C/2 h/vac coatings with 30 at.% Al, which were likely γ'-$(Fe,Ni)_3Al$.

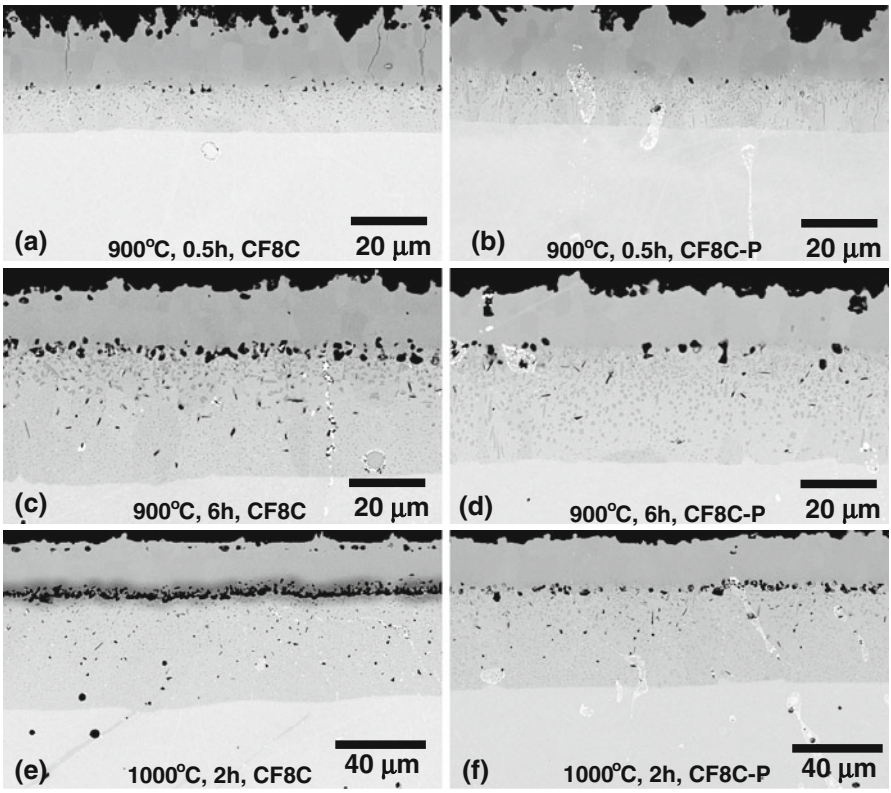

Fig. 1 BSE images of metallographic sections of as-annealed slurry aluminide coatings on alloys CF8C and CF8C-P. Annealing conditions and alloys were: **a** CF8C, 900 °C/0.5 h/vac, **b** CF8C-P, 900 °C/0.5 h/vac, **c** CF8C, 900 °C/6 h/vac, **d** CF8C-P, 900 °C/6 h/vac, **e** CF8C, 1,000 °C/2 h/vac, **f** CF8C-P, 1,000 °C/2 h/vac

Table 2 Comparison of layer thickness and composition for selected coatings

Test condition	Substrate alloy	Coating type	Slurry anneal temp. (°C)	Slurry anneal time (h)	OL Avg. thickness (μm)	IDZ Avg. thickness (μm)	Total Avg. thickness (μm)	Coating Avg. Al (at.%)	IDZ Avg. Al (at.%)	Coating Avg. Cr (at.%)	IDZ Avg. Cr (at.%)
Green	CF8C-P	Green slurry	NA	NA	126 ± 12	NA	126	100	NA	NA	NA
Annealed, vac	CF8C	Slurry	1,000	2	28.2 ± 3.2	52.7 ± 1.7	86	36 ± 2.7	8.2 ± 3.5	9.5 ± 2.2	20.4 ± 1.5
Annealed, vac	CF8C-P	Slurry	1,000	2	23.9 ± 1.8	48.1 ± 1.4	72	29.8 ± 3	8.2 ± 4.6	11.2 ± 2	22.6 ± 1.7
Annealed, vac	CF8C	Slurry	900	0.5	17.5 ± 2.6	12.0 ± 0.7	36	49.4 ± 2.4	9.6 ± 7.9	8.5 ± 1	21.6 ± 0.9
Annealed, vac	CF8C-P	Slurry	900	0.5	19 ± 3.7	13.8 ± 0.7	33	48.3 ± 3.1	14.2 ± 8.3	9 ± 1.1	22.3 ± 3.5
Annealed, vac	CF8C	Slurry	900	6	15.9 ± 3.7	34.6 ± 1.6	54	32.5 ± 3.4	9.2 ± 4.4	10.3 ± 2.4	20.9 ± 1.3
Annealed, vac	CF8C-P	Slurry	900	6	19.5 ± 3.3	30.5 ± 1.8	50	34.4 ± 2.2	9.3 ± 5.3	10.5 ± 1.8	22.4 ± 1.7
As-CVD	CF8C-P	CVD	900	6	4.5 ± 0.4	30.4 ± 0.3	35	38.5 ± 5	12.2 ± 9.3	6 ± 4	19.6 ± 4.6
As-aluminized	CF8C-P	Pack	900	6	7.2 ± 0.7	37.5 ± 1.4	45	41.4 ± 0.2	11.6 ± 8.7	6.3 ± 2.6	20.4 ± 3.5
3 kh @ 800 °C	CF8C-P	Slurry	900	6	17.4 ± 2.2	67.7 ± 7.6	85	6 ± 3.9	5.7 ± 1.6	16.8 ± 1.3	22.7 ± 1.4

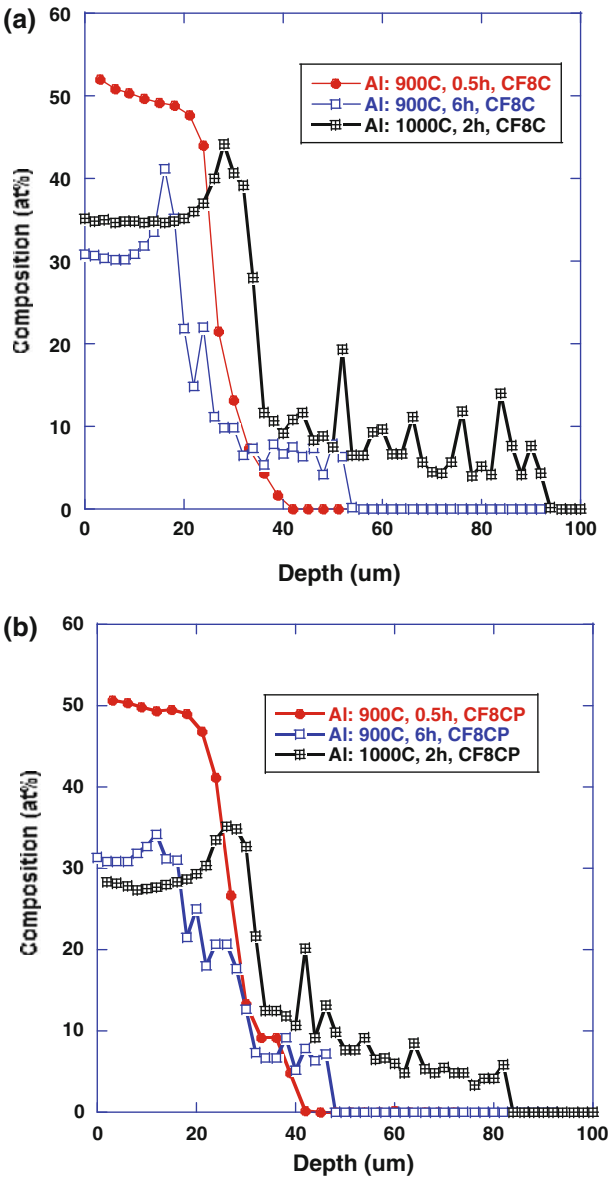

Fig. 2 Electron microprobe line profiles from various as-fabricated slurry coatings comparing the Al content from the coating surface into the stainless steel alloy. **a** As-fabricated coatings on alloy CF8C. **b** As-fabricated coatings on alloy CF8C-P

Variations in heat treatment, and to a lesser degree alloy content, had an impact on both coating structure and composition. Figure 2a (CF8C) and b (CF8C-P) compare Al line profiles across the slurry coating thickness after annealing at the three different conditions shown in Fig. 1. Higher annealing temperatures and

longer times resulted in thicker coatings (i.e., deeper penetration of Al), as expected. The Al content of the OL decreased as temperature and/or time increased, due to more rapid inward diffusion of Al and outward diffusion of Fe/Ni. The Al content of the OL after 2 h at 1,000 °C on alloy CF8C (Fig. 2a) was higher than that of the same coating on CF8C-P (Fig. 2b). The difference in Al content was attributed to the eventual inhibition of Al diffusion toward the alloy by the near continuous layer of porosity along the OL–IDZ interface on CF8C (Fig. 1).

Selected elemental maps of as-fabricated slurry coatings (900 °C, 6 h) on CF8C and CF8C-P are compared in Figs. 3 and 4. The matrix of the IDZ was depleted in Ni, an austenite stabilizer, and enriched in Al and Cr, both ferrite stabilizers. The

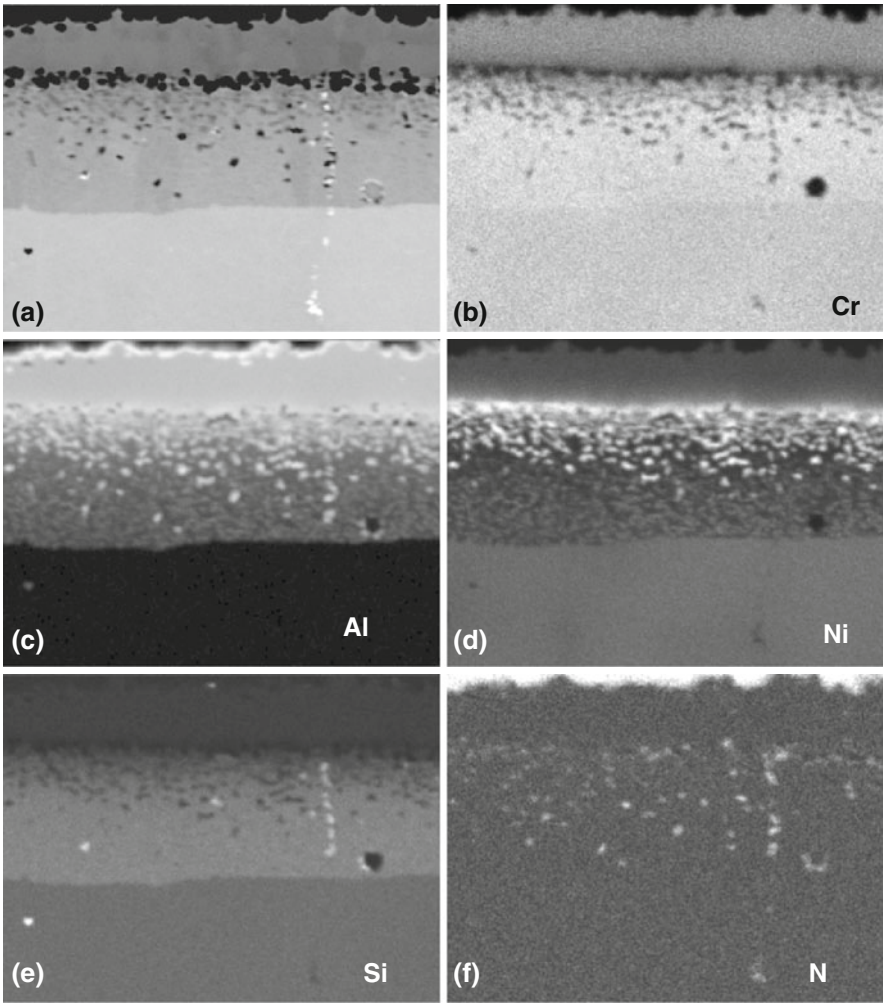

Fig. 3 X-ray maps of as-annealed (900 °C/6 h) slurry aluminide coating on alloy CF8C. **a** BSE image, **b** Cr map, **c** Al map, **d** Ni map, **e** Si map, **f** N map

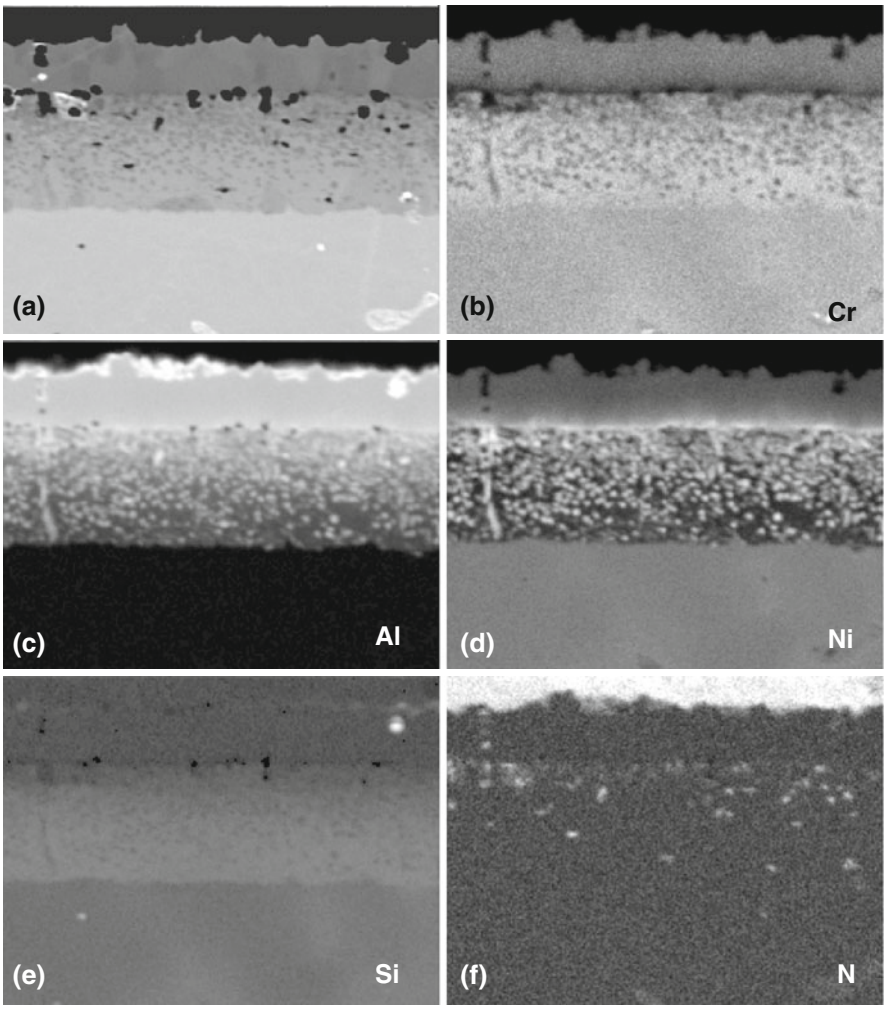

Fig. 4 X-ray maps of as-annealed (900 °C/6 h) slurry aluminide coating on alloy CF8C-P. **a** BSE image, **b** Cr map, **c** Al map, **d** Ni map, **e** Si map, **f** N map

IDZ of the as fabricated coatings contained 8–14 at.% average Al (Table 2). The maps and Al concentrations suggest the original austenite alloy structure transformed to BCC ferrite within the IDZ, as a result of austenite destabilization due to the high concentration of Al, as also reported in previous studies [9, 11, 18]. The Ni-rich precipitates within the IDZ are β-NiAl in the ferrite matrix, agreeing with similar observations in a previous analytical microscopy study of the IDZ on a 310 stainless steel [9]. Coatings on CF8C-P contained greater quantities of NiAl precipitates (Fig. 4d) than the base CF8C alloy (Fig. 3d), likely due to the higher Ni content of CF8C-P (Table 1).

The ferritic IDZ also contained a non-uniform dispersion of small AlN precipitates (some acicular, some rounded), as indicated by the N maps in Figs. 3f

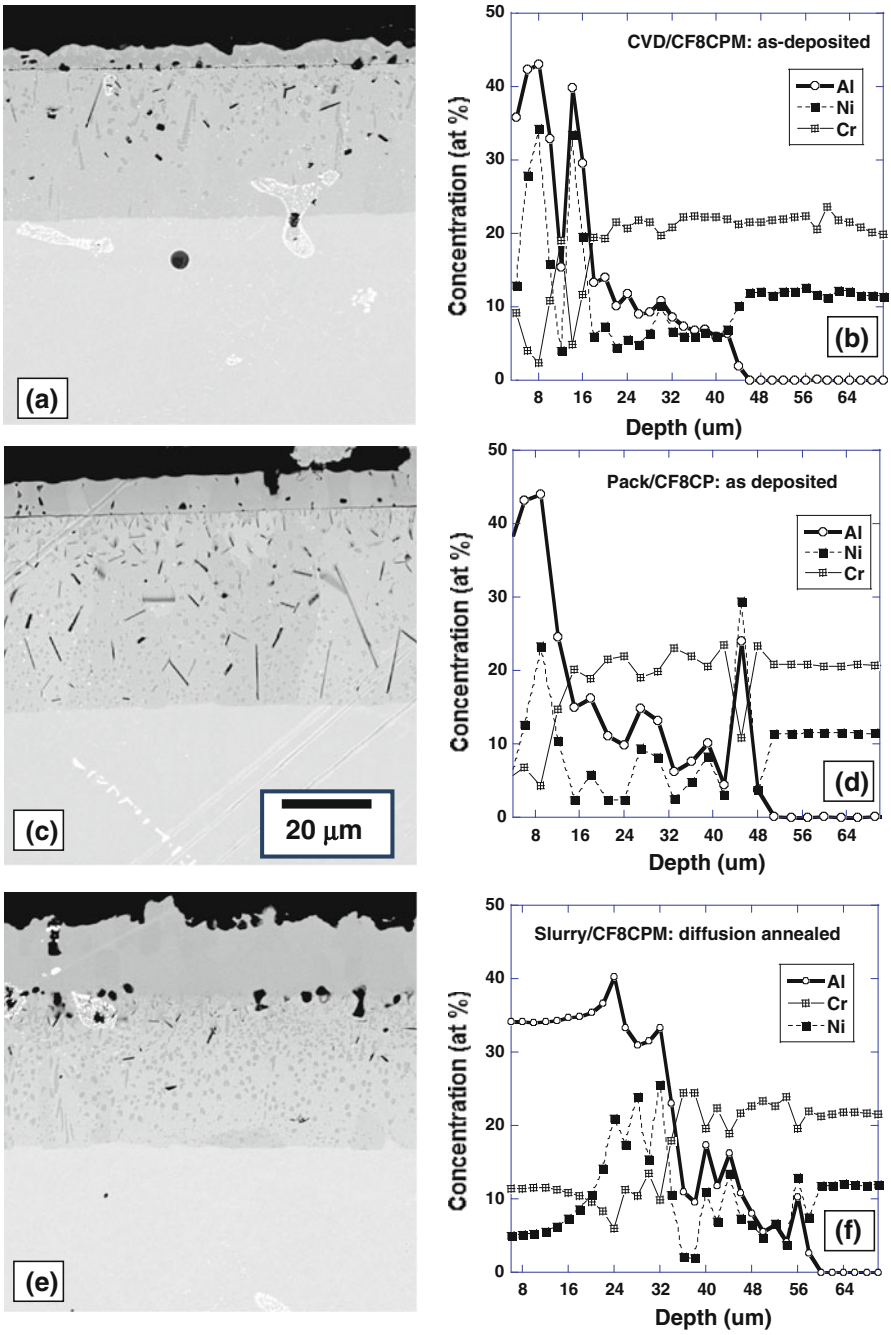

Fig. 5 BSE images and EPMA composition profiles (Al, Cr and Ni) of the three types of diffusion aluminide coatings fabricated at 900 °C for 6 h on stainless steel alloy CF8C-P: **a**, **b** CVD coating with average Al content of 39 at.% on alloy CF8C-P, **c**, **d** PC coating with average Al content of 41 at.% on alloy CF8C-P2, and **e**, **f** ORNL slurry coating with average Al content of 34 at.% on alloy CF8C-P

and 4f, the images in Fig. 5, and as reported elsewhere [21]. Thus, the aluminide coating inherently reduces the near-surface N content of the alloy by forming AlN. Formation of AlN precipitates is important, since the unusually high creep and rupture resistance of CF8C-P type alloys is dependent on maintaining an appropriate dispersion of stable NbC nano-carbides and Nb/Cr nano-nitrides [1, 2].

Characterization of As-Fabricated CVD and Pack Aluminide Coatings

Comparative aluminide coatings were also fabricated by low activity CVD (on alloys CF8C and CF8C-P) and PC on alloy CF8C-P. Figure 5a–f compares BSE images of metallographic sections of coatings by CVD, PC, and slurry aluminizing, alongside their respective EPMA concentration profiles of Al, Cr and Ni. Each type of coating in Fig. 5 was processed for 6 h at 900 °C. All three types of coatings had a single-phase β-(Fe,Ni)Al OL (Table 2) and an underlying ferritic IDZ containing β-NiAl and AlN precipitates. Table 2 compares the thickness and average Al and Cr contents of each layer, with OL average Al contents ranging from 34 to 41 at.% for the three coatings.

The 900 °C/6 h CVD process (Fig. 5a, b) resulted in the thinnest OL and least total coating thickness (~5 and 35 μm, respectively). Thickness and average Al composition (39 at.%) were nearly identical to those reported on CVD aluminized 304L stainless steel [16]. However, the same CVD aluminizing process on a 9-Cr martensitic–ferritic alloy resulted in a total coating thickness of ~53 μm [16], illustrating the slower inward Al diffusion that occurs in the closer packed FCC structure of an austenitic steel. The CVD coating on CF8C-P contained moderate amounts of porosity along the OL–IDZ interface, and was rich in Ni compared to the slurry and PC coatings (Fig. 5b). The higher Ni content (Fig. 5b) is at least partly due to of the low Al activity CVD process, resulting in Ni diffusing outward more rapidly than Al diffuses inward.

The OL and total thickness (~7 and 45 μm, respectively) of a 900 °C/6 h PC coating on a CF8C-P alloy from a previous heat with a slightly different composition (7.8 at.% Ni, 1.8 at.% Mn) (Fig. 5c) were greater than that of the CVD coating as a result of the higher Al activity of the pack process. The average composition of the OL was ~41 at.% Al (Table 2), with a moderate increase in Ni over the alloy composition, as shown in the EPMA profile of Fig. 5d.

In comparison to the pack coatings, the OL thickness and total thickness (~20 and 50 μm, respectively) were further increased for the 900 °C/6 h/slurry coating on CF8C-P (Fig. 5e). The average Al content of the OL was ~34 at.%, with only the inner region of the OL enriched in Ni (Fig. 5f). The total thickness (OL + IDZ) for the pack and slurry coatings in Fig. 5 was similar (~50 μm). The OL–IDZ interface was the least defined for the slurry coating, as compared to the distinct linear interfaces visible for the CVD and PC coatings. Additionally, the slurry coatings had the roughest and most irregular surfaces of the three coating types.

Oxidation Testing of Bare CF8C-Plus Alloys

Figure 6a compares the oxidation mass changes of bare coupons of CF8C-P at 700 °C in air + 10 % H_2O, 750 °C in air + 10 % H_2O and 800 °C in both dry air

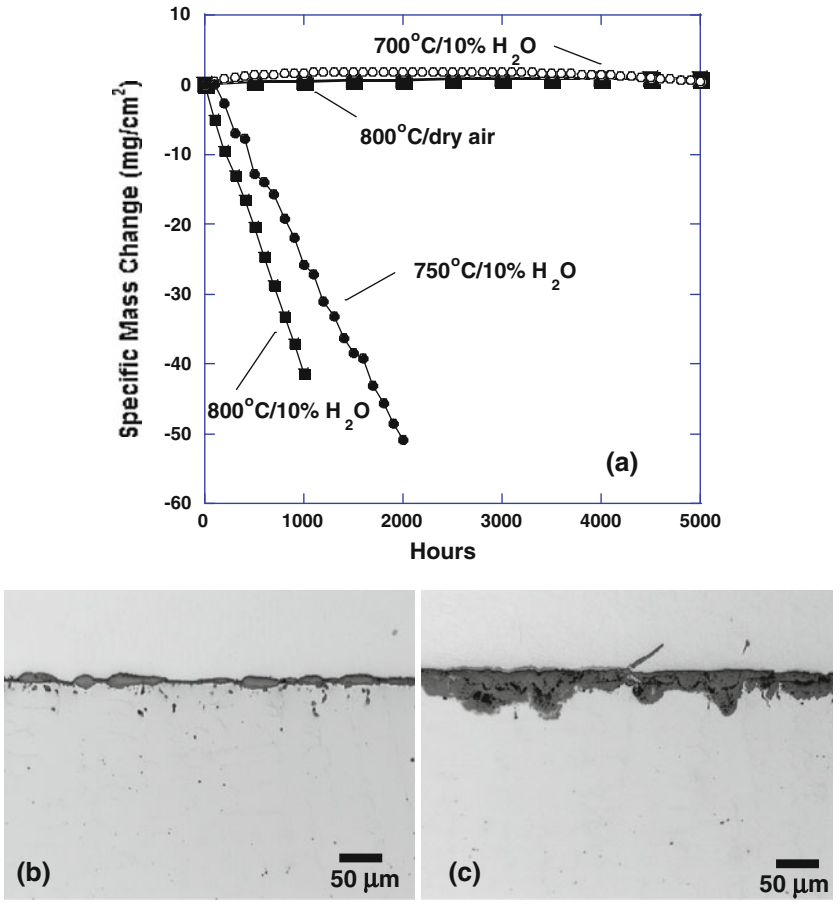

Fig. 6 **a** Oxidation mass changes for bare CF8C-P alloys cycled (100 h cycles) at 700, 750 and 800 °C in dry air and/or air + 10 % H_2O. **b** Optical image of metallographic section of bare alloy CF8C-P after 5 kh oxidation at 800 °C in dry air, and **c** bare alloy CF8C-P after 1 kh in air + 10 % H_2O at 800 °C

and air + 10 % H_2O. At 700 °C in H_2O the bare alloy formed a stable, Cr_2O_3-based scale, with only a modest amount of spallation after 5 kh. But at 750 °C in H_2O, the alloy no longer maintained a protective scale, resulting in rapid and continuing mass loss due to progressive oxide spallation and re-formation (and perhaps scale volatility). The rate of mass loss was even more rapid in water vapor at 800 °C. However, at 800 °C dry air, a slow-growing, stable oxide scale was maintained after 5 kh. These results illustrate the potentially significant impact of water vapor on scale adherence as temperatures increase, particularly for a Cr_2O_3-forming alloy with lower Ni content, such as CF8C-P.

The optical photos in Fig. 6b, c compare the microstructures and thickness of the oxide scale (mostly Cr_2O_3) formed on CF8C-P1 after 5 kh oxidation in dry air at 800 °C (Fig. 6b) to the scale formed after 1 kh in air + H_2O at 800 °C (Fig. 6c). Scale thickness and depth of oxidation attack in Fig. 6c were much greater after one

fifth the exposure time in water vapor, illustrating the need for a protective coating on CF8C-P in the presence of water vapor at 750 °C and higher.

Oxidation Testing of Coated CF8C and CF8C-Plus Alloys

Figure 7 compares the cyclic oxidation behavior (100 h cycles) of various slurry, CVD and PC coatings on alloys CF8C and/or CF8C-P at 800 °C in air + H_2O. The CVD aluminide coatings on both alloys showed similar semi-parabolic mass gains with no signs of mass loss after 3 kh. Surface analysis by SEM showed an adherent alumina scale with occasional clusters of small Mn- and/or Cr-rich oxides. There was no evidence of oxide cracking or spalling, other than at coupon corners, after 3 kh. One PC aluminide coating on CF8C-P was tested for 1 kh (Fig. 7). A small mass loss occurred after 500 h. There was a steady mass gain afterwards, indicating that the coating remained protective after 1 kh. The original rate of mass gain was similar to the CVD coatings.

Slurry coatings (annealed at 900 °C 6 h) on both CF8C and CF8C-P were tested to 3 kh (Fig. 7). The 900 °C/6 h slurry coating on CF8C exhibited a very similar oxidation curve to the CVD coatings. Figure 8a, b shows SEM images of the coating surface on CF8C after 3 kh, indicating an adherent alumina scale, covered with uniformly spaced, bright-contrast oxide "flowers" rich in Mn and/or Cr (and Fe in some locations), as determined by EDS. There was no evidence of significant oxide spalling after 3 kh. Figure 9 shows a replicate coating (900 °C/6 h) on CF8C tested for 2 kh, with a very similar oxidation curve. It should be noted that the slurry coating specimens had rough, irregular surfaces, as well as occasional cracking and porosity. Thus, the mass gains per surface area have a substantial error, since there is a much greater actual surface area than what was calculated based on a smoother

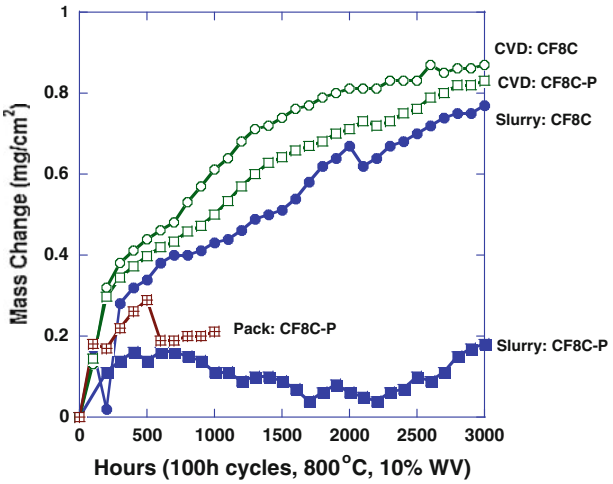

Fig. 7 Cyclic oxidation (100 h cycles) at 800 °C in water vapor for slurry aluminide coatings on CF8C and CF8C-P, compared to CVD coatings on the same alloys and a PC coating on CF8C-P. All aluminide coatings in this figure were fabricated at 900 °C for 6 h

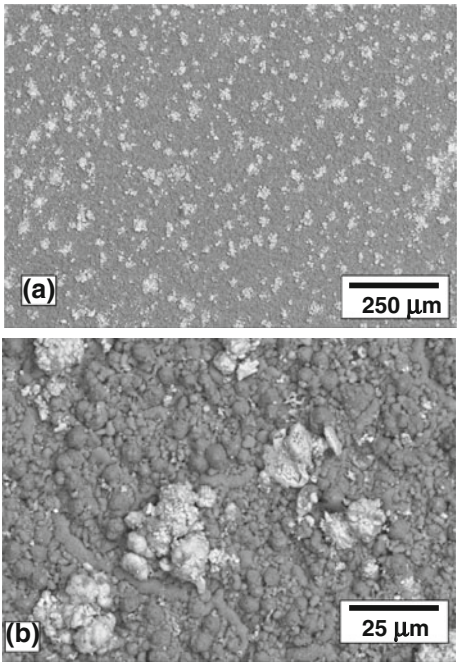

Fig. 8 BSE images of the surface of a slurry aluminide coating (900 °C/6 h) on cast alloy CF8C after 3 kh cyclic oxidation at 800 °C in air + 10 % H_2O (Fig. 7). **a** Plan view of typical surface showing no spallation of oxide, and bright-contrast oxide "flowers" on the alumina scale. **b** Mn-rich oxide nodules on the alumina surface

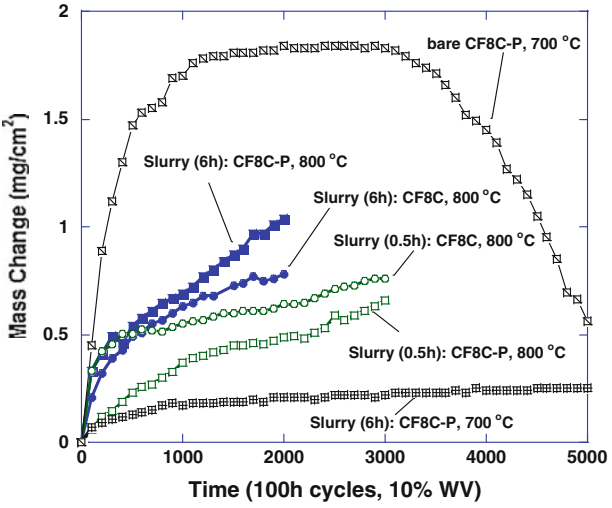

Fig. 9 Cyclic oxidation (100 h cycles) at 700 or 800 °C in water vapor. All slurry coatings on CF8C or CF8C-P alloys were fabricated at 900 °C, with slurry annealing times of either 0.5 or 6 h shown in parentheses in the figure labels above. Both of the 900 °C, 6 h specimens tested at 800 °C are replicates of the slurry coating in Fig. 7a. The bare CF8C-P alloy is provided for comparison to the slurry coating tested at 700 °C

coupon surface (such as a bare alloy or CVD or pack coating). Thus, the actual comparative rate of oxide growth per surface area is lower for the slurry coatings than is apparent in Figs. 7 and 9.

The 900 °C/6 h slurry coatings on alloy CF8C-P displayed greater variability in oxidation mass change behavior (Fig. 7). The specimen in Fig. 7 had small amounts of spallation initiating at ~500 h, while afterward maintaining a positive but irregular mass curve to 3 kh. The replicate 900 °C/6 h slurry coating on CF8C-P (Fig. 9) exhibited a steady mass gain to 2 kh, with no evidence of mass loss. Figure 10a, b shows SEM surface images of the 900 °C/6 h slurry coating (Fig. 7) on CF8C-P after 3 kh. The majority of the surface was adherent alumina, with occasional isolated small, oxide particles rich in Mn and Cr (Fig. 10a). The exception was a large semi-circular region with a very high concentration of oxide particles and whiskers (Mn- and Cr- and Fe-rich) on one side of the test coupon. Figure 10b is from the perimeter of that region, showing the abrupt transition from a primarily alumina scale to a scale overlaid with a high density of brighter-contrast oxide particles. There was evidence of minor scale spallation and re-growth in the affected region, explaining the continuing minor mass losses in Fig. 7. However, most of the remaining surface was covered with adherent Al_2O_3 (Fig. 10a). It is possible that there was a processing-related coating irregularity in this localized area resulting in reduced scale adherence.

Slurry coatings annealed at 900 °C for a shorter time (0.5 h) on CF8C and CF8C-P exhibited steady oxidation mass gains, with the coating on CF8C-P having the lowest mass gain of all coatings tested at 800 °C after 3 kh, as shown in Fig. 9.

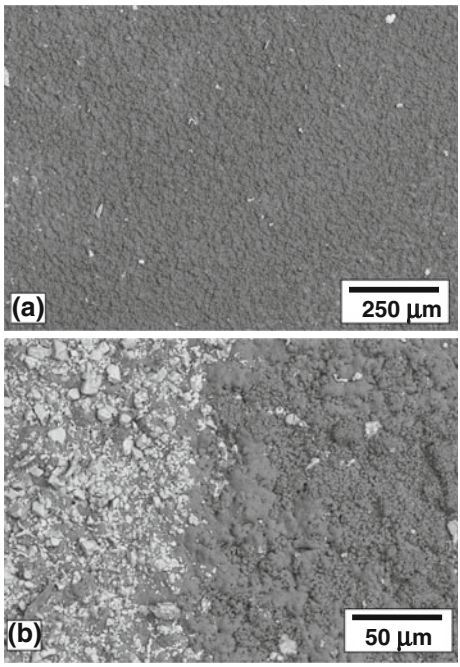

Fig. 10 BSE images of the surface of a slurry aluminide (900 °C/6 h) on cast alloy CF8C-P after 3 kh cyclic oxidation at 800 °C in air + 10 % H_2O (see Fig. 7a). **a** Plan view of a representative surface showing the typical uniform, adherent alumina scale. **b** Transition area from alumina to the localized zone where the alumina surface was decorated with bright-contrast Mn-rich oxide particles and whiskers. Most of the specimen surface had the appearance of (**a**)

There was no evidence of significant oxide spallation. Although there were occasional oxide "flowers" rich in Mn and Cr, they were much less plentiful than those shown in Fig. 8b, thus explaining the lower mass gains. These slurry coatings had the thickest OL, highest Al content (Figs. 1, 2), and most cracking, due to their brief aluminizing anneal not allowing time for substantial interdiffusion of Al and Fe/Ni.

Figure 9 also compares two specimens cyclically oxidized (100 h cycles) at 700 °C in air + 10 % H_2O. The bare CF8C-P alloy was tested to 5 kh, and exhibited a modest mass gain for a Cr_2O_3-forming alloy. The bare alloy began to exhibit a gradual mass loss after approximately 3 kh, most likely due to oxide spallation. A slurry coated (900 °C, 6 h) CF8C-P alloy was also tested to 5 kh. This coating showed an extremely low rate of mass gain, since it formed alumina. There was no evidence of oxide spallation from the slurry coating after 5 kh at 700 °C.

Characterization of 3 kh Oxidized Slurry Coating Cross-Section

The 900 °C/6 h slurry coating specimen on alloy CF8C-P was characterized via metallographic analysis of coating microstructure and composition after 3 kh oxidation testing (Fig. 7). Figure 11a, b compares BSE images of this specimen. There were occasional through-cracks in the OL, but no crack propagation into the IDZ was observed. These through-cracks typically contained a thin layer of alumina due to oxidation and served as short-circuit diffusion paths resulting in moderate oxidation of most of the pre-existing pores along the OL–IDZ interface (Fig. 11a).

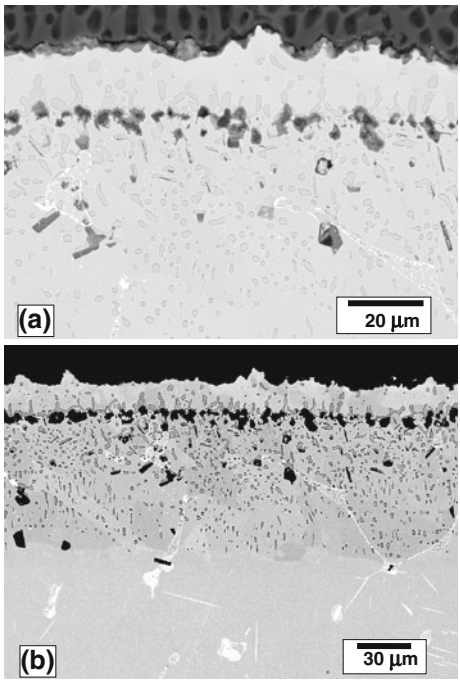

Fig. 11 BSE images of metallographic sections of slurry aluminide coating (900 °C/6 h) on CF8C-P after 3 kh cyclic oxidation at 800 °C in air + 10 % H_2O

The oxidized surface exhibited a relatively thin (2.3 ± 1.2 μm), uniform surface scale (Fig. 11a). There were occasional secondary oxides rich in Cr or Mn in the scale cross-section, but the scale was primarily alumina. The OL had an average remaining thickness of 17.4 ± 2.2 μm and exhibited a non-uniform, 2-phase structure, consisting of an Al-depleted matrix containing vertically elongated Ni–Al particles with higher Al content than the OL matrix. The Ni–Al particles, which were likely the remnants of the original coating phase, show up as the medium contrast particles in Fig. 11, and were primarily located near the IDZ interface. Numerous smaller precipitates of similar contrast, presumed to be β-NiAl, were uniformly distributed throughout the IDZ, which had increased in thickness from ~31 to 68 μm (Table 2). There were also occasional long stringers of brighter-contrast Nb carbides in the IDZ (Fig. 11b), some spanning the thickness of the IDZ. The IDZ contained modest quantities of elongated, blocky or acicular AlN particles (the dark contrast particles in Fig. 11), most of which were located nearer the OL interface, and a few of which were near 10 μm in length (Fig. 11a).

The lower magnification optical photo in Fig. 12 shows the complete coupon cross-section with intact coating visible on both surfaces. This image demonstrates that slurry coating oxidation behavior was relatively uniform across the coupon after 3 kh.

Figure 13 compares the Al and Cr profiles obtained by EPMA line scans across the thickness of the slurry coating after 3 kh. During high temperature exposure, the original Al in the OL was lost via at least four mechanisms: (1) oxidation of the surface, (2) local spallation and re-formation of the surface oxide, (3) oxidation of the interface, and (4) diffusion into the underlying substrate. The average compositions (Al and Cr) and thickness values of the OL and IDZ in the region of the line traces after 3 kh oxidation are listed in Table 2. As expected, Al contents were substantially reduced. Average remaining Al content in the OL after 3 kh was 6 ± 3.9 at.%, as compared to 34.4 ± 2.2 at.% in the as-annealed coating (Table 2). It was concluded from the EPMA results that the majority of the OL had transformed into a ferritic (BCC) structure with similar composition to the IDZ, but also containing large remnant particles of β-NiAl and/or γ-Ni_3Al. The oxidized coating still had more than adequate average Al and Cr to continue to form alumina, especially considering the beneficial secondary element effect of 14–16 % Cr. Most of the Ni–Al was depleted from the near-surface region after 3 kh.

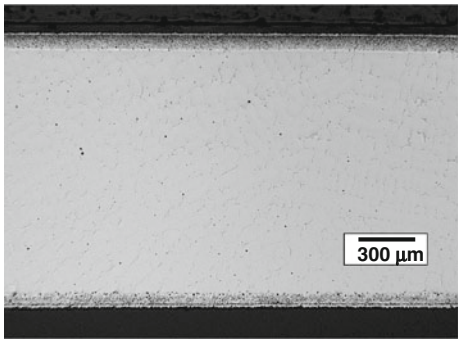

Fig. 12 Optical image of complete metallographic cross-section of a slurry aluminide coating (900 °C, 6 h) on CF8C-P after 3 kh oxidation testing at 800 °C in 10 % WV

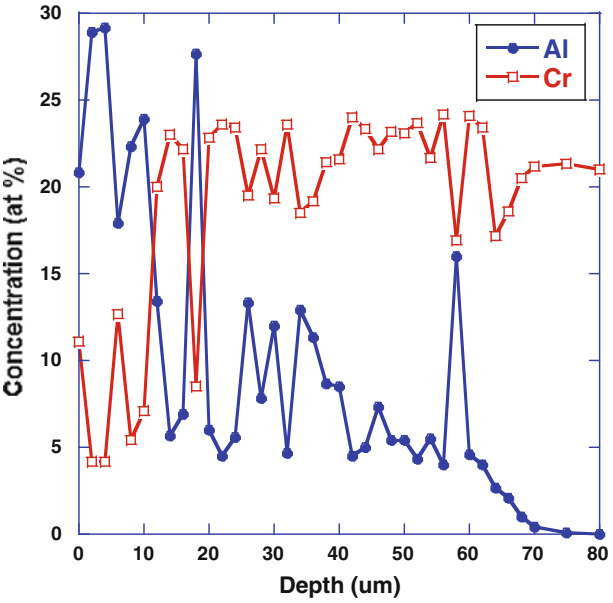

Fig. 13 EPMA line profiles across the coating after 3 kh oxidation testing at 800 °C of a simple slurry aluminide coating (900 °C/6 h) on alloy CF8C-P, comparing Al and Cr concentrations

Table 3 Electron microprobe of slurry coatings before and after 3 kh Oxidation AT 800 °C (compositions in at.%)

Slurry coating	Alloy type	Coating condition	Analysis location	Fe	Cr	Ni	Al	Mn	Si	Nb
900 °C/6 h	CF8C-P	0 h	OL surface[a]	48.1	11.9	5.5	31.3	2.8	0.2	0.1
			OL average[b]	44.7	11.1	9.7	31.6	2.6	0.2	0.1
			IDZ average	53	20.5	8.3	12.9	3	1	0.1
900 °C/6 h	CF8C-P	3 kh	OL surface[a]	66	16.5	8.8	3.6	3.9	0.8	0.2
			OL average[b]	62	16.8	10.3	6.0	3.9	0.7	0.1
			IDZ average	57.1	22.7	8.5	5.7	3.3	0.8	0.8

[a] Point scan in aluminide OL immediately below surface

[b] Average of line scan in aluminide OL

Table 3 compares the measured EPMA compositions in the OL at the point immediately beneath the coating surface, as well as the composition for major elements averaged across both the OL thickness and the IDZ thickness, for the 0 h and 3 kh 900 °C/6 h slurry coating. The Al content of the lower-Al matrix phase was ~3.6 at.% just beneath the oxide scale. There was little gradient in Cr across the OL in the 0 h or 3 kh coating, with average content increasing from 11.1 at 0 h to 16.8 at.% at 3 kh. The Cr content of the IDZ increased from 20.5 to 22.7 at.%. There was also little gradient in Mn across the OL in either condition, with average content increasing from 2.6 at 0 h to 3.9 at.% at 3 kh, with very little change in the

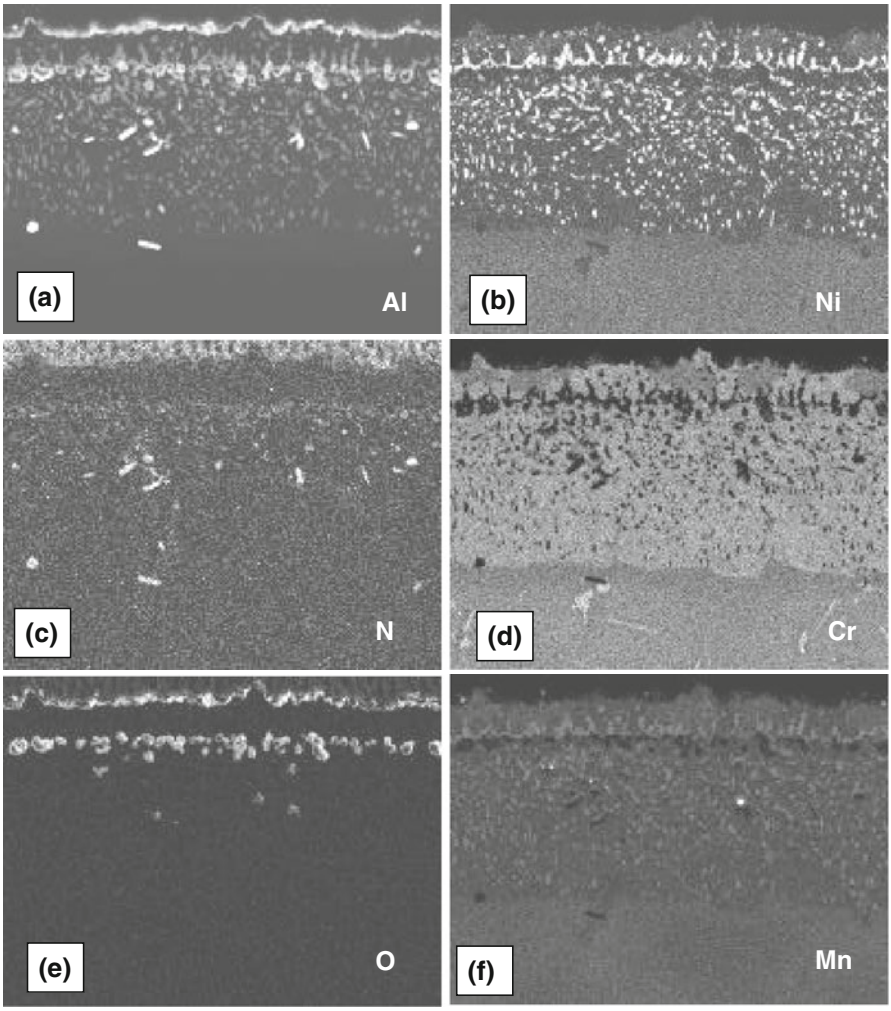

Fig. 14 X-ray maps of cross-section of aluminide slurry coating (900 °C/6 h) on CF8C-P after 3 kh oxidation testing at 800 °C in 10 % H_2O

IDZ after 3 kh. The average Nb content of the IDZ increased significantly after 3 kh, but that was likely related to the non-uniform presence of Nb carbides throughout the alloy at both 0 and 3 kh.

Figure 14 shows elemental maps (Al, Ni, Cr, N, Mn and O) for the 900 °C/6 h/CF8C-P specimen after 3 kh. The Ni map in Fig. 14b shows a significant concentration of NiAl precpitates remaining in both the OL and IDZ. The maps also show that the peak in Al near the OL–IDZ interface in Fig. 13 was related to Ni–Al particles. The Mn map shows no Mn-rich oxides, indicating that diffusion of Mn or Cr through the oxide scale to form oxide surface particles was not ubiquitous, even with high Mn contents in the coating. Al was detected to a depth of $\sim$110 μm.

By comparison, an Al diffusion depth of ~270 μm and an average Al content of 4 at.% Al in the surface layer were reported for a CVD aluminide on stainless steel alloy 304L after 6 kh at 800 °C in air + 10 % H_2O [11]. In contrast, an Al diffusion depth of over 750 μm was measured for a CVD aluminide coating on a ferritic-martensitic 9-Cr alloy after 6 kh in the same 800 °C test [11]. There appears to be an obvious advantage in aluminizing austenitic alloys, since the solubility of Al is much lower in austenite and thus inward diffusion of Al is slower, resulting in more gradual depletion of Al from the coating and IDZ. This comparison suggests that much longer lifetimes for quality aluminide coatings on austenitic alloys could be anticipated, particularly at temperatures lower than 800 °C.

Low Cycle Fatigue Testing of Aluminized CF8C-Plus

Figure 15 compares the fatigue life of the uncoated, slurry coated and pack-cementation coated CF8C-P specimens. For comparison purposes the fatigue lives of uncoated samples annealed at 0.5 and 1 h at 900 °C prior to fatigue testing are also shown. Taking into account the obvious caution that these are single specimen comparisons at the present time, the preliminary observations from this figure are:

(i) The diffusion annealing treatment appeared to result in substantial improvements in the fatigue life of alloy CF8C-P. This is evident from the fact that the fatigue life of the annealed samples was ~100 and ~125 % higher than that of the uncoated sample.

(ii) The fatigue life of the thin slurry coating (900 °C/0.5 h) was ~160 % higher than that of the uncoated as-cast sample, which was 60 % higher than that which could be accounted for by the improvement occurring due to the annealing treatment. Analysis of this result suggested that this additional improvement in fatigue life may have been due to the superior oxidation resistance of the thin coated sample as compared to the bare sample [22].

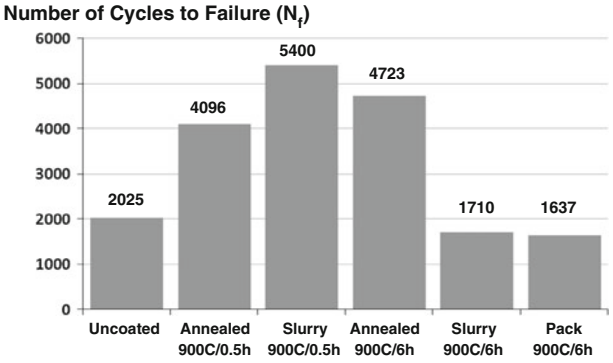

Fig. 15 Comparison between the fatigue lives of uncoated and coated samples of CF8C-P. The coating type and aluminizing process and the number of cycles to failure, N_f are listed on the plot. The samples were fatigued under fully reversed strain-controlled mode ($R = -1$) at 800 °C with total strain range of 0.5 % and strain rate of 0.05 % 1/s in laboratory air. The two specimens listed as annealed were uncoated

(iii) The fatigue life of the thick coatings (slurry at 900 °C/6 h, pack at 900 °C/6 h) was ~10 to 20 % lower than the uncoated sample. This result suggested that the effective stiffness and the strain energy available for macro-crack initiation may have increased due to the higher thickness of the more brittle coating layers. This effect may overshadow the improvement in fatigue life due to the heat treatment [22].

Significant further fatigue testing, perhaps in a subsequent program, will be necessary to draw firm conclusions.

Discussion

Multiple types of simple slurry aluminide coatings on cast austenitic stainless steel CF8C-P displayed robust oxidation resistance during aggressive cyclic oxidation testing at 800 °C in water vapor. Bare alloys showed extensive scale spallation under these test conditions after tens of hours. Within the 3 kh maximum duration of testing in this study, the low cost slurry aluminide coatings provided oxidation resistance at least equal to that of CVD aluminides. All versions of slurry coatings appeared at least equal to that of the pack coating. The excellent durability of the slurry coatings was somewhat unexpected considering that the slurry was simple Al, and had not been optimized for austenitic alloys. However, the CF8C-P alloy (which does not require an annealing treatment after casting) allowed a higher temperature slurry anneal, thus enabling lower coating Al contents and better thermo-mechanical stability than would be expected for slurry aluminide coatings annealed at lower temperatures.

Previous studies of slurry coatings, generally with higher Al contents than those in this study, have primarily been evaluated on ferritic steels. A commercial slurry aluminide on a 9-Cr steel was reported to form non-protective Fe–O, after testing for 1 kh at 650 °C in steam, a result attributed to improper surface preparation [10]. In contrast, Agüero et al. [15] has shown >40 kh lifetime for aluminide slurry coatings on 9-Cr alloys at 650 °C in steam. This comparison illustrates that proper coating selection and processing for a specific alloy and environment are crucial to enable consistently successful coating performance.

Slurry coating durability and failure mode under the present test conditions is still unknown, due to both the robust nature of the coatings and the limited scope and duration of this study. Pint and Zhang [19] report that CVD aluminide coatings fabricated by CVD on 304L have survived over 6 kh testing at 800 °C, and 20 kh testing at 700 °C, both in 10 % water vapor. The slurry coating tested at 700 °C in this study showed no signs of degradation after 5 kh. The 800 °C oxidation results in this study suggest that these slurry aluminides, with higher total Al content (due to their greater thickness) may have comparable or superior lifetime to the CVD aluminides.

It is likely that coating failure will ultimately be driven by eventual Al depletion, combined with accelerated formation of Mn- and Cr-rich oxides. The average Al content of OL after 3 kh testing was 6 at.% (Table 2), with an average Cr content of

16.8 at.%. In comparison, Kvernes et al. [23] reported that only 2.1 at.% Al was needed for resistance to water vapor at 680 °C in an alloy with 13 % Cr. Increasing Cr content and oxidation temperature are both known to reduce the critical Al content necessary to maintain a protective Al_2O_3 scale. Critical Al contents as low as 0.5–1.1 at.% have been reported for CVD aluminide coatings on 9-Cr ferritic-martensitic alloys at 800 °C [11].

It's also important to note that the average Al content of the thicker underlying IDZ was 5.7 at.% after 3 kh as compared to 6 at.% in the OL (Table 2). Once the Al content of the OL drops beneath that of the IDZ, it is possible that the Al in the IDZ will serve as an Al reservoir to "feed" the depleted OL with Al, maintaining it at or above the critical level until the IDZ is also depleted of Al. This would be most feasible for coatings with a non-continuous oxide layer along the OL–IDZ interface. Thus, it is possible that the most valuable coating assets for long term corrosion resistance on austenitic alloys could prove to be the Al content of the thicker IDZ, combined with the Cr content of the OL. Thus, Cr content of the austenitic alloy is likely to be a critical factor for long-term coating performance, particularly at higher temperatures or more aggressive conditions.

Preliminary testing suggested that the impact of a diffusion aluminide coating on the fatigue life of CF8C-P at 800 °C can vary from mildly detrimental to beneficial, depending on coating thickness. However, much more fatigue data is needed before any firm conclusions can be drawn. It will be important to continue to develop a much more comprehensive understanding of aluminide coating impact on the fatigue and creep properties of high temperature steels.

It will be of interest to also evaluate slurry aluminide oxidation performance on CF8C-P alloys (as well as other high temperature austenitic steels) for much longer durations in the temperature range of 700–800 °C. Previous long-term diffusion studies of CVD aluminide coatings on 304 stainless steel showed negligible Al diffusion at 600 °C (no reduction in Al content after 10 kh), moderate diffusion at 700 °C (Al decreasing from 26 to 20 at.% after 5 kh), and significant interdiffusion at 800 °C (Al decreasing from 25 to 12 at.% after 2 kh) [24]. These diffusion studies, combined with the present 800 °C oxidation study, suggest that high quality β-(Fe,Ni)Al slurry aluminide coatings on austenitic steels have potential to be protective for tens of thousands of hours at 700–750 °C.

Conclusions

It was demonstrated that multiple types of aluminide coatings (CVD, pack and slurry) can provide effective oxidation protection for cast CF8C-P austenitic steels under aggressive oxidation testing conditions (air + 10 % H_2O), with slurry coatings remaining protective and stable after 3 kh at 800 °C and 5 kh at 700 °C. A variety of slurry aluminide coatings—with varying thickness and Al content—were tested, most of which showed excellent oxidation resistance at 800 °C. The microstructure, composition, porosity and phase content of the slurry coatings varied with processing, and there were indications that substrate composition had an influence on coating porosity. All slurry coatings showed good thermo-mechanical

compatibility with the alloy, with only modest cracking and no coating failures after up to 3 kh.

Preliminary fatigue tests of uncoated, coated and bare heat treated specimens indicated that a thick coating degrades the LCF life of the alloy by 10–20 % at 800 °C, whereas a thin coating improved the fatigue life by ~60 %, likely due to improved oxidation resistance. In light of these results it is suggested that it will be important to develop an understanding of the long-term impact of the coating and annealing treatments on the mechanical properties, especially the creep and fatigue resistance, of CF8C-P and other high temperature alloys.

Appropriately designed low-cost slurry aluminide coatings appear to be a viable long-term option for oxidation protection of CF8C-P and other austenitic alloys in water vapor/steam. They seem particularly attractive for development for long-term applications in the range of 700 or 750 °C, where oxidation rates, Al diffusion rates and Al depletion rates would be substantially reduced over those in the present 800 °C study.

Results of this study reinforce the important point that a coating, alloy and specific environment must be evaluated and compared as a system. One size coating does not fit all, and identical coatings can show wide variation in performance with differing alloys and environments. That physical reality can become a design advantage if the coating user understands this sensitivity, or a disadvantage if not.

Acknowledgments The authors would like to thank L. Walker, J. Henry, K. Cooley, and M. Howell for their role in the experimental work. S. Pawel provided helpful comments on the manuscript. This work reported in this manuscript has been performed by UT-Battelle, LLC, under contract with the U.S. Department of Energy. The research was sponsored by the U.S. Department of Energy, Office of Energy Efficiency and Renewable Energy, Industrial Technology Program.

References

1. P. J. Maziasz, J. P. Shingledecker, N. D. Evans and M. J. Pollard, *Journal of Pressure Vessel Technology* **131**, 051404-1 (2009).
2. P. J. Maziasz, J. P. Shingledecker, N. D. Evans, and M. J. Pollard, *Advanced Materials Process* **166**, 27 (2008).
3. P. J. Maziasz and B. A. Pint, *Journal of Engineering for Gas Turbines and Power* **133**, 1 (2011).
4. J. P. Shingledecker, P. J. Maziasz, N. D. Evans and M. P. Pollard, *International Journal of Pressure Vessels and Piping* **84**, 21 (2007).
5. J. P. Shingledecker, P. J. Maziasz, N. D. Evans, M. L. Santella and M. P. Pollard, *Energy Materials: Materials Science & Engineering for Energy Systems* **1**, 25 (2006).
6. H. Asteman, J. E. Svensson, L. G. Johansson and M. Norell, *Oxid. Met.* **52**, 95 (1999).
7. Y. Zhang, B. A. Pint, J. A. Haynes and P. F. Tortorelli, *Oxid. Met.* **62**, 103 (2004).
8. J. L. Smialek and C. E. Lowell, *Journal of the Electrochemical Society* **121**, 800 (1974).
9. N. V. Bangaru and R. C. Krutenat, *Journal of Vacuum Science & Technology* **4**, 806 (1984).
10. R. N. Durham, L. Singheiser and W. J. Quaddakers, *Materials Corrosion* **59**, 402 (2008).
11. B. A. Pint and Y. Zhang, *Materials Corrosion* **61**, 1 (2010).
12. D. Kumar, B. A. Pint, S. Dryepondt, B. L. Armstrong, Y. Zhang, A. Shyam, J. A. Haynes, and E. Lara-Curzio, *Performance of Diffusion Aluminide Coatings Applied on Alloy CF8C-Plus at 800°C, Corrosion 2011 Proceedings* (NACE International, Houston, TX, 2011).
13. A. Agüero, J. Garcia de Blas, R. Muelas, A. Sanchez and S. Tsipas, *Materials Science Forum* **369–372**, 939 (2001).
14. A. Agüero, R. Muelas, A. Pastor and S. Ogersby, *Surface and Coatings Technology* **200**, 1219 (2005).

15. A. Agüero, R. Muelas, M. Gutiérrez, R. Van Vulpen, S. Osgerby and J. P. Banks, *Surface and Coatings Technology* **201**, 6253 (2007).
16. Y. Zhang, B. A. Pint, K. M. Cooley and J. A. Haynes, *Surface and Coatings Technology* **202**, 3839 (2008).
17. Y. Zhang, B. A. Pint, G. W. Garner, K. M. Cooley and J. A. Haynes, *Surface and Coatings Technology* **188–189**, 35 (2004).
18. B. A. Pint, Y. Zhang, L. R. Walker and I. G. Wright, *Surface and Coatings Technology* **202**, 642 (2007).
19. B. A. Pint and Y. Zhang, *Materials and Corrosion* **62**, 549 (2011).
20. B. A. Pint and J. M. Rakowski, NACE Paper 00-259, Houston, TX (Presented at NACE Corrosion 2000, Orlando, FL, March 2000).
21. A. Agüero and R. Muelas, *Materials Science Forum* **461–464**, 957 (2004).
22. D. Kumar et al., *Mater. Sci. Eng. A*, to be submitted (2013).
23. I. Kvernes, M. Olivera and P. Kofstad, *Corrosion Science* **17**, 237 (1977).
24. Y. Zhang, A. P. Liu and B. A. Pint, *Materials Corrosion* **58**, 751 (2007).